

**GLOBAL COMPOSITIONAL CARTOGRAPHY OF PLUTO FROM LEISA DATA.** L. R. Gabasova<sup>1</sup>, B. Schmitt<sup>1</sup>, W. Grundy<sup>2</sup>, C. B. Olkin<sup>3</sup>, J. R. Spencer<sup>3</sup>, L. A. Young<sup>3</sup>, K. Ennico<sup>4</sup>, H. A. Weaver<sup>5</sup>, S. A. Stern<sup>3</sup>, and the New Horizons Composition Team; <sup>1</sup>Université Grenoble Alpes, CNRS, IPAG (Grenoble, France, [leila.gabasova@univ-grenoble-alpes.fr](mailto:leila.gabasova@univ-grenoble-alpes.fr)), <sup>2</sup>Lowell Observatory (Flagstaff, AZ, USA), <sup>3</sup>SwRI (Boulder, CO, USA), <sup>4</sup>NASA Ames Research Center (Mountain View, CA, USA), <sup>5</sup>JHU-APL (Laurel, MD, USA).

**Introduction:** The July 2015 flyby of the Pluto system by the NASA New Horizons mission returned a wealth of data, greatly advancing our knowledge of its surface topography, geology, and composition, as this is the first time we have been able to observe and map it directly. The highest-resolution data is limited to the encounter hemisphere of Pluto, but lower-resolution images obtained during the approach allow for the production of global mosaics.

Schmitt et al. [1] gives a comprehensive qualitative analysis of the spatial distribution of the various materials present on the surface of the encounter hemisphere. N<sub>2</sub> and CH<sub>4</sub> ices are present both separately and in a ternary molecular mixture with CO ice, as is H<sub>2</sub>O ice and a dark red organic material. While extending this study globally is possible via the lower-resolution approach images, pointing imprecisions result in several degrees of misregistration between the encounter and approach datasets, necessitating additional co-registration before global mosaics can be created.

Schenk et al. [2] produced a panchromatic global reflectance map using both the LORRI framing camera and the MVIC panchromatic channels, and Earle et al. [3] co-registered the MVIC colour channel images to the LORRI map. The high-resolution LEISA data has also been registered to the panchromatic map using feature-based methods. These methods, however, have proven inadequate for registering the LEISA approach imagery, as the imaging distance combined with the lower resolution of the instrument result in there not being any readily identifiable feature edges in the far hemisphere.

A class of methods that is promising for this kind of data is intensity-based registration, which involves comparing intensity patterns in the images to be registered. Different metrics can be used to evaluate their similarity, such as cross-correlation, mutual information, or sum of squared intensity differences. Intensity-based registration is a very common tool in medical imagery processing, and is very easily adapted to planetary data.

**Methods:** We process 12 approach cubes in order to have complete global coverage, with native pixel resolutions ranging from 30 to 354 km/px. The highest-resolution of these is registered using the closest-approach high-resolution data as a target image and each subsequent cube is registered to the one above it

in resolution order (e.g. second-highest resolution to highest, third-highest to second-highest, etc.). This is done to maximise overlap between the source and target images and provides overall more accurate registration, despite the risk of error propagation.

The LEISA hyperspectral datacubes are captured over a short time, which means the same transformation matrix will be applicable to all wavelengths. This means we can calculate the transformation matrix using a subset of the datacube — one which features large contrasts and clear patterns — and apply it to all the other wavelengths. The CH<sub>4</sub> ice map produced by [1] using the integrated band depth of the 1.7 μm band group has precisely these properties, and serves as the basis for the registration.

We apply intensity-based registration algorithms from ITK (Insight Segmentation and Registration Toolkit, an open-source library). As we expect the misalignment between the datasets to be due entirely to imprecisions in the spacecraft pointing information, we restrict ourselves to global similarity transformations (i.e. translation, rotation, and scale). We use an evolutionary algorithm-based optimiser and a Mattes mutual information metric [4].

**Results:** We verify the registration accuracy using a small number of control points based on identifiable features (shown in Figure 1) as well as visual comparison with the global panchromatic reflectance map. The six highest-resolution approach maps registered accurately to better than 1 pixel of each map's native resolution. Due to the lack of a spectrally-analogous anchor on the opposite hemisphere, some latitudinal drift occurred for the next six maps. This was corrected manually and will be automated in a future iteration of the algorithm.

Figures 2–4 show the global maps for the CH<sub>4</sub> integrated 1.7 μm band depth, the H<sub>2</sub>O spectral index, and the red material spectral index. The N<sub>2</sub> and CO spectral index maps will also be shown at the meeting.

**Discussion:** The global CH<sub>4</sub> map allows us to confirm the presence of a methane belt in the 0–30°N latitude range, extending globally beyond the bladed terrains seen in the high-resolution images [5]. The macula region covering most of Pluto's surface between 0–30°S is also quite clearly visible in the global red material map.

These are the first global registered composition maps of the surface of Pluto, allowing us to study the correlation of composition with geological features on

the non-encounter hemisphere. They also provide a cartography of volatiles for radiative transfer models, and will allow the calculation of latitudinal and longitudinal means of  $N_2$ ,  $CH_4$ , and  $CO$ , from which we can obtain the global radiation budget of Pluto in 2015. These maps also provide useful inputs and constraints for global circulation models to study the origin of the current ice distribution of Pluto.

**References:** [1] B. Schmitt, et al. *Icarus*, 287:229–260, 2017. [2] P. M. Schenk, et al. *Icarus*, 314:400–433, 2018. [3] A. M. Earle, et al. *Icarus*, 314:195–209, 2018. [4] D. Mattes, et al. In *Medical imaging 2001: image processing*, volume 4322, pages 1609–1621. SPIE, 2001. [5] J. M. Moore, et al. *Icarus*, 300:129–144, 2018.

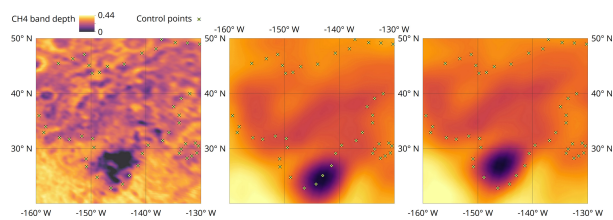


Figure 1: Example of intensity-based registration results for the Pluto  $CH_4$   $1.7 \mu m$  band depth map, showing the Pulfrich crater area. Left: high-resolution image, centre: unregistered lower-resolution image (native resolution 30 km/px), right: registered lower-resolution image.

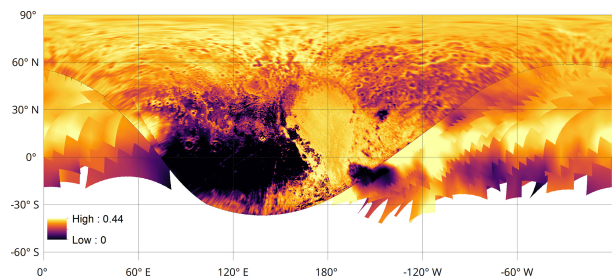


Figure 2: Global registered  $CH_4$  map ( $1.7 \mu m$  integrated band depth).

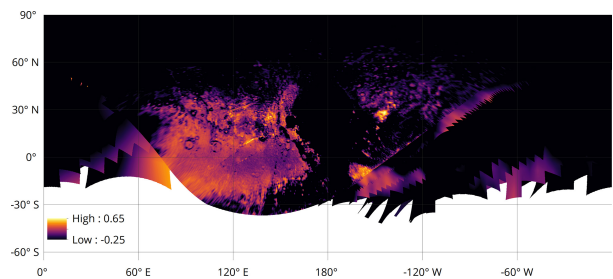


Figure 3: Global registered  $H_2O$  spectral index map.

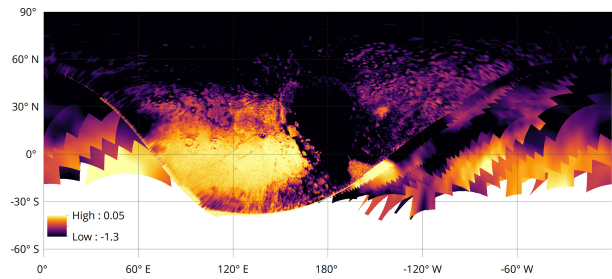


Figure 4: Global registered red material spectral index map.